

# A Framework for Operational Volume Generation for UAM Strategic Deconfliction

Ellis L. Thompson<sup>1</sup> and Yan Xu<sup>2</sup> and Peng Wei<sup>3</sup>

**Abstract**—Strategic pre-flight systems focus on the planning and deconfliction of routes for aircraft systems. The urban air mobility concept calls for higher levels of autonomy with both onboard and en route systems but also strategic and other pre-flight systems. Existing endeavors into strategic pre-flight systems focus on improving the route generation and strategic deconfliction of these routes. Introduced with the urban air mobility concept is the premise of operational volumes, 4D regions of airspace, including time, a single aircraft is expected to operate within, forming a contract of finite operational volumes over the duration of a route. It is no longer enough to only deconflict routes within the airspace, but to now consider these 4D operational volumes. To provide an effective all-in-one approach, we propose a novel framework for generating routes and accompanying contracts of operational volumes, along with deconfliction focused around 4D operational volumes. Experimental results show efficiency of operational volume generation utilising reachability analysis and demonstrate sufficient success in deconfliction of operational volumes.

## I. INTRODUCTION

Urban Air Mobility (UAM) concept is generally described in [1]–[3] as: a safe and efficient, highly automated, aviation transportation infrastructure, for passengers and cargo, operating at low altitudes. The highly automated nature of this concept favors emerging technologies for aircraft, such as Unmanned Aircraft Systems (UASs) and electric Vertical Take-Off and Landing (eVTOL) vehicles, as well as Air Traffic Management (ATM) and route planning systems. The European Aviation Safety Authority (EASA) predict UASs to become prevalent in European cities by 2025 [2], and the Federal Aviation Administration (FAA) estimates 828 thousand unmanned commercial aircraft by 2024 [4].

The prediction of high-density UAM air space brings with it the requirement for both highly automatized aircraft and ATM techniques. Introducing autonomy at the strategic pre-flight, level can provide efficient route planning and deconfliction for aircraft agents wishing to enter the airspace. Additionally, autonomous air vehicles and ATM systems can provide tactical instructions to ensure the airspace remains safe with efficient traffic flow.

A UAM operator is introduced as an entity responsible for the management of UAM specific operations [5]. A UAM

service provider therefore is any entity offering services to assist with or provide UAM operations. One such role that either an operator or service provider is responsible for is route planning and sufficient deconfliction for safe and efficient flight. The concept of four-dimensional (4D) regions of airspace, including time, is presented as Operational Volumes (OVs) [6], [7], with the intention that those operating aircraft remain within their designated OVs for the duration of the flight. This consequently becomes an agreed upon contract between the aircraft operator and airspace, of where the aircraft is allowed to operate and for what duration.

In this paper we propose a novel approach to generating semi-deconflicted routes and accompanying contracts of OVs for aircraft. We build our definition of OVs on that proposed in SkyTrakx [8], with adaptations made to provide a more adaptive approach with the intention of a tactical deconfliction layer added in-flight to ensure safety of aircraft. Our approach uses reachability analysis to generate OVs based on the simulated behavior of aircraft. In our approach we also propose a rapidly-exploring random tree (RRT) based algorithm for two-dimensional (2D) route generation and build the OVs simultaneously, providing constraints during the route generation.

The remainder of this document is formatted as following: Section II, examines works related to OV generation, reachability analysis and route generation and deconfliction. Sections III and IV, outline the approaches used for constructing contracts of OVs and route generation; Experiments and evaluations on the approaches used are outlined in V. A discussion on the work presented is in Section VI. Finally, a conclusion and the direction of future work is provided in Section VII.

## II. RELATED WORKS

### A. Concept of Operations

Guidelines for the approach for traffic management within the UAM concept are outlined in [6], [7], [9], [10]. The FAA, NASA, and EUROCONTROL's SESAR joint undertaking group each provide high-level outlines on the direction for the management and operational standards of aircraft in the UAM airspace. Namely, the concept of OVs are referenced as regions of airspace for the aircraft agents to remain in throughout the duration of a flight.

### B. Route Planning

Route planning algorithms provide potential candidate routes from an origin to a destination. Shortest path algorithms, such as Dijkstra's algorithm, A\* and D\* [11]–[13],

<sup>1</sup>Ellis L. Thompson is with the School of Engineering and Applied Science, George Washington University, Washington, DC 20052, USA [thompson\\_e@gwu.edu](mailto:thompson_e@gwu.edu)

<sup>2</sup>Yan Xu is with the Centre for Autonomous and Cyberphysical Systems, Cranfield University, Bedford, MK43 0AL, UK [yanxu@cranfield.ac.uk](mailto:yanxu@cranfield.ac.uk)

<sup>3</sup>Peng Wei is with the School of Engineering and Applied Science, George Washington University, Washington, DC 20052, USA [pwei@gwu.edu](mailto:pwei@gwu.edu)

provide a shortest path through a series of nodes through the optimisation of some cost or heuristic function. Additionally, the classification of RRT based algorithms [14]–[17] provide a randomized approach to path finding distinct from a shortest path approach. Of the two, D\* [13] and rapidly-exploring random tree fixed nodes - dynamic (RRT\*FND) provide the ability to alter routes in a changing environment, these dynamic approaches prove potentially viable for the dynamic UAM environment. Examples of route planning approaches for Unmanned Aerial Vehicle (UAV)/UAS applications are given in [18]–[21].

### C. Strategic Deconfliction

Strategic Deconfliction [22] concepts focus primarily on pre-flight stratagem to ensure a conflict free environment or decrease the likelihood of en route conflict states. Route planning and re-planning can be encompassed in strategic deconfliction but with a greater emphasis on re-planning for conflict resolution. Operating either spatially in three-dimensional (3D) space or temporally as well in 4D space, strategic deconfliction systems, such as [23]–[25], can provide deconflicted routes where the probability of near mid-air collisions is reduced pre-flight.

### D. Reachability Analysis

Reachability analysis is the process of computing reachable sets given some initial conditions. Common in the verification space, DryVR [26] provides a suite for generating reachable sets and evaluating the validity of them through learning a discrepancy function and related sensitivities. Alternatives to reachability analysis and reach tube generation are presented in [27]–[29], focusing on a lagrangian approach to optimal reach tube generation, whereas [30], [31] provide bloating techniques.

### E. Operational Volumes, Geofences and SkyTrakx

SkyTrakx [8] proposes an approach to generating a contract of OV's for a route and specific aircraft type by performing a reachability analysis over a finite time horizon. The SkyTrakx framework demonstrates the application of reachability-based OV generation, for light UASs, for both rotor and fixed-wing aircraft. They further allow for two generation types of OV's: conservative and aggressive, with the latter producing tighter bounded OV's. Dynamic geofences are also proposed in [32] for coordination of low-altitude UASs. In [19], the approach to route generation also includes the concept of building *keep-in* geofences, regions of airspace a UAS controller should endeavor to ensure the drone remains within. Alternative approaches to geofence use and generation are also presented in [33], [34].

## III. CONTRACTS AND OPERATIONAL VOLUMES

In this section we provide definitions for the terms *contract* and *operational volume*, as well as provide our three-step method for generation a contract of 4D OV's utilising the DryVR [26] framework.

### A. Defining Contracts and Operational Volumes

An OV is a 4D region of airspace that, in the context of this work, describes the operating airspace of an aircraft from sometime  $t_0$ , and for duration  $t_d$ . The initial time  $t_0$ , relative to an OV conveys the time that the OV becomes active. Consequently,  $t_d$ , in relation to an OV, is the duration that the OV remains active. More formally, we adapt the definition of an OV from that given in SkyTrakx [8] (Equation 1).

$$C = (R_1, T_1), (R_2, T_2), \dots, (R_k, T_k) \quad (1)$$

The definition of an OV ( $C$ ) given in Equation 1, is a finite sequence of pairs  $(R_i, T_i)$  where  $R_i \subseteq X$ ,  $X \subseteq \mathbb{R}^3$  is a subset of the airspace and  $T_i$  is monotonically increasing time. Duration ( $t_d$ ) is the time prescribed that the OV should exist for where,  $t_d = T_k - T_1$ . The total airspace of the OV is defined in Equation 2 as the union of all  $R_i$ s.

$$C_{\text{airspace}} = \bigcup_{i=1}^k R_i \quad (2)$$

By extension, a contract ( $\Sigma$ ) is a set of all OV's. An extension we make to the definition of a contract given in SkyTrakx [8], allows for an overlap ( $t_{\text{offset}}$ ) between adjacent OV's in the same contract. where,  $k$  is the number of OV's in  $\Sigma$ , the duration of the contract then becomes:

$$\Sigma_{\text{dur}} = t_d k - t_{\text{offset}}(k - 1) \quad (3)$$

Rather than the duration of the contract ( $\Sigma$ ), being the combined duration of all OV's in that contract, because of the introduced, fixed-time overlap ( $t_{\text{offset}}$ ), this needs to be accounted for.

Furthermore, as is outlined in Section IV, this definition deviates yet further from SkyTrakx. Where overlapping, time-aligned OV's in different contracts violate the safeness of the proposed SkyTrakx approach, in our approach overlaps are permitted. This is due to leveraging the requirement for aircraft to continuously make progress through their route. In return, this requirement produces the ability to represent an aircraft's position within an OV probabilistically. To achieve this a representation of aircraft positional data at each time step is also stored with the OV data and modify Equation 1 accordingly, where  $D$  now represents the distribution of aircraft positional data at the corresponding time step.

$$C = (R_1, T_1, D_1), (R_2, T_2, D_2), \dots, (R_k, T_k, D_k) \quad (4)$$

### B. Generating Operational Volumes

For a given, predefined route, OV's are generated using an adaptation of the DryVR [26] framework. Included within the DryVR framework is: "a probabilistic algorithm for learning sensitivity of the continuous trajectories from simulation data" as well as an algorithm that then uses these sensitivities to perform a reachability analysis and, generating a reach tube. We leverage these algorithms in conjunction with the BlueSky [35] ATM simulator, to generate simulated aircraft traces, to generate a contract of 4D OV's.

The DryVR framework requires a series of simulator trajectories to perform the reachability analysis. As such, and to ensure sufficient uncertainty is maintained in the simulation, OVs are generated iteratively in three steps: (1) Uncertainty is introduced into the simulation through the initialization of agent starting states; (2) The simulation is run, for some duration ( $t_d$ ) with agent states being stored at regular intervals (e.g. 1 second); (3) The DryVR framework is used on a sample of output trajectories and then verified on the remaining trajectories. This three-step approach is repeated until the agents have reached the terminal waypoint in the simulation. The resultant OVs are then combined into a contract.

1) *Initializing aircraft states with uncertainty:* To introduce variation and uncertainty into the simulation  $N$  agents, between 500 and 2000 are created. For the first initialization, i.e., from the origin waypoint, the position, altitude, heading and speeds are chosen at random from between predetermined bounds.

After each simulation run to  $t_d$ ,  $N$  new aircraft are initialized in the system. Unlike the initial run however, these positions are sampled from the previous batch of trajectories, more specifically, they are sampled from the normal distribution of states from some offset  $t_{offset} \pm c$ , where  $c$  is some time constant in seconds. This approach favors generating states closer to the existing *mean state* but provides some uncertainty and variation. Additionally, to avoid potentially infeasible states from occurring, the samples are bound to lie either within the previous OV or no further than some fixed distance  $c$  from the OV.

2) *Collecting trajectory data from the simulation:* From the initialized states the BlueSky simulation is run for the duration  $t_d$ . The step-size and log interval are independent of each other and in our environment are 0.1 seconds and 1 second respectively. Two aircraft were used in our simulations: an Amazon octocopter available through the OpenAP [36] suite and the Airbus Vahana eVTOL vehicle using performance data available in [37], [38]. These aircraft provide two different examples of UAM space users to run evaluations on, although, they are not used together when generating OVs.

For  $N$  agents in the environment  $S_N$  states were generated each second. Each state stores: record time, latitude, longitude, altitude, heading, vertical speed (m/s), true airspeed (m/s). Noise was also added to the values in the state to further inject uncertainty. The positional data (latitude and longitude) as offset in a random direction by a random amount chosen from the interval  $[3m, 15m]$ . All others, except the record time, had random noise applied, chosen from the interval  $[-5, 5]$ .

The result of the second phase is  $N$  trajectories ( $T_N$ ) where the states of the  $N$  agents are taken at 1 second intervals up to  $t_d$ .

3) *Generating OVs from trajectories:* The resultant trajectories from the simulations are then used in the DryVR framework to perform reachability analysis and obtain the resultant reach tube. These reach tubes, in conjunction with

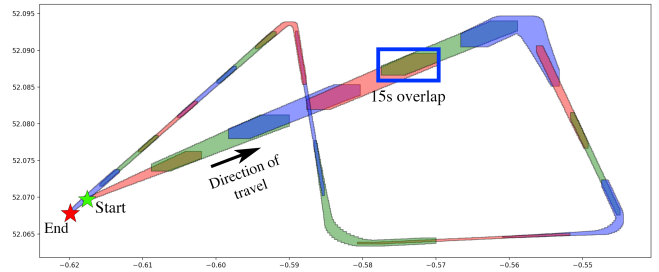


Fig. 1: A two-dimensional, top-down view of the 18 OVs in a contract. The duration ( $t_d$ ) of each OV is 60 seconds and a 15 second offset has been used. Each OV has been given a color (red, green or blue) to easily distinguish them.

additional metadata describing the distribution of the aircraft positions used to generate the OV, then represent individual OVs which in turn build contracts.

The reachability analysis is performed in 3D space over the current and next states for each time step. As such, for all trajectories only the: record time, latitude, longitude and altitude are provided to the framework. To avoid over or under estimation for trajectories with a small geographical footprint, the latitude, longitude and altitude are normalized.

The DryVR framework is provided with a subset of 15-20 trajectories  $T_X \subset T_N$ . Additionally, the center trajectory ( $T_X^{center}$ ) is provided and is used by DryVR to generate the sensitivities. The remaining set ( $T_N - T_X$ ) is used for verification of the OV to ensure accuracy and sufficient inclusion of trajectories.

The output of the framework is a reach tube which, combined with  $t_d$  and initialization time ( $t_0$ ), create a single OV. The OVs can then be combined into a contract spanning the proposed flight path as seen in Fig. 1.

### C. Distribution of Aircraft within OVs

Aircraft are expected to make constant progression along their route, this is derived from the finite time that an OV, and by extension a contract, can exist (Equation 3). As such, and to ensure efficient use of the airspace when generating routes, the position of an aircraft within an OV can be represented as a probability distribution at time  $t$ , and then utilised in route planning to avoid regions of airspace with high probabilities.

As provided in Equation 4, the definition of an OV includes  $D_t$  for the distribution of aircraft positional data at time  $t$ . As, for any given position  $S \in C$ , the probability of a simulated aircraft existing at  $s$  is virtually 0. Therefore, the value is instead representative of the probability of an aircraft existing in an  $N \times N$  area, within the bounds of  $C$ , resulting in  $m \times n$  finite regions. We use  $C^{m,n}$  to denote an individual  $N \times N$  meter area.

Where  $S$  is a position to query such that there is a function  $f(S) \mapsto (m,n) \in C$ , then the respective probability of an aircraft existing in any given  $N \times N$  meter region at time  $t$  can be given as Equation 5.

$$P(S, t, C) = \frac{\sum a_t \in C^{m,n}}{\sum a_t \in C} \quad (5)$$

#### IV. ROUTE GENERATION

In this section we cover our approach to route generation using a modification of the RRT\* algorithm outlined in [16] RRT\*FND. We also outline the joint process of building deconflicted routes, where the OVs generated in section III are deconflicted with others in the airspace.

##### A. An Overview of RRT\*FND and RRT-Rope

1) *RRT\*FND*: The RRT\*FND algorithm [16] was chosen as a path planning algorithm due to its ability to perform well in dynamic environments. Built on the *fixed node* concept of rapidly-exploring random tree fixed nodes (RRT\*FN) [15], RRT\*FND can generate routes between two points in an environment with dynamic obstacles.

RRT\* firstly builds routes through randomly adding nodes into an environment and then re-wiring the tree such that the cost from the origin node to any other node is minimized, with respect to all the nodes in the tree. This is referred to as the *GROW* function and forms the base of RRT\*FND. Operating identically to RRT\*, RRT\*FN introduces the concept of *fixed nodes*, that is a maximum number of nodes ( $M$ ) that can exist in the tree. The tree uses *GROW* until the number of nodes exceeds  $M$  when RRT\*FN employs a force removal algorithm. The algorithm, in short, randomly selects a childless node to remove from the tree so that the number of nodes in the tree remains no greater than  $M$ . There is a possibility that the last node on the solution path is childless. If this is the case, then it is excluded from the force removal algorithm as to not risk destroying or impairing the solution.

RRT\*FND improves RRT\*FN for dynamic environments by utilizing existing information if the solution path is severed. RRT\*FND introduces the *Reconnect* and *Regrow* functions. If the existing solution path is severed, *Reconnect* attempts to reconnect the last node directly to the solution tree. If this connection cannot be made, then *Regrow* attempts to connect the main tree to any node in the solution tree.

2) *RRT-Rope*: RRT-Rope [17] shortens existing paths using a short cutting technique similar to pulling a rope. This was added to, in addition to shortening a path, provide a smoother path, easier for an aircraft to follow.

For each node in the solution tree, it looks at every subsequent node, starting with the furthest node first. It evaluates is a direct path has any collision with the environment. Providing no collision is found the two nodes will be connected by a straight line. Intermediate nodes are then added between the two points completing the shortening.

##### B. Utilisation of RRT\*FND

1) *Preprocessing*: To ensure consistency with the RRT\*FND algorithm, specifically consistency with distances, the airspace area was first converted to a grid with

cells of constant width. The latitude and longitude coordinates were converted to xy-coordinates using Equations 6-7, to obtain meters per degree of latitude/longitude at the latitude  $\phi$  [39], [40].

$$111132.92 - 559.82 \cos 2\phi + 1.175 \cos 4\phi + 0.0023 \cos 6\phi \quad (6)$$

$$111412.84 \cos \phi - 93.5 \cos 3\phi + 0.118 \cos 5\phi \quad (7)$$

2) *Generating Routes*: In the UAM airspace we expect regions of static No-Fly Zones (NFZs). Described in [33] as “keep-out” geofences, the NFZs are regions of airspace that the route generation must never overlap with. Additionally, generated OVs must not have any overlap with the NFZ regions of airspace to ensure aircraft will not enter them as part of the prescribed contract.

In addition, with static NFZs routes should maintain sufficient deconfliction with OVs within other contracts. Unlike NFZs however, OVs only exist for a finite duration ( $t_d$ ) and so, from the perspective of the RRT\*FNDs algorithm, appear as dynamic obstacles appearing and disappearing with the progression of time. Futhermore, unlike NFZs, to ensure efficient use of airspace, some overlap of OVs in different contracts is permitted, ensuring the total cost of the overlap remains below a threshold, the utilization of this is provided in Section IV-C.

Routes are therefore generated following the aforementioned RRT\*FNDs algorithm, running until a valid solution is generated. Once a solution has been realized the route is optimized for distance using a modified RRT-Rope [17] algorithm. As the airspace could be dense and optimizing the route could incur a higher computational cost an optimization factor is applied to the modified RRTs-Rope *tightening*. This value describes how many points to consider for the optimization, where a higher value results in a more direct route, this is demonstrated in Fig. 2.

After a candidate solution is generated the OV generation begins. After each OV has been generated the aircraft positions, boundaries and associated times are compared with both the NFZs and OVs in other contracts for violations, more context on what constitutes an overlapping violation is given in Section IV-C. If a violation is found, violating nodes are removed from the graph and the *Reconnect* and *Regrow* functions of RRT\*FND are used to dynamically reconnect the graph. The RRT-Rope approach is used to optimize the route for distance on the newly added segment only. Finally, the OV generation is performed from the last valid OV segment.

##### C. Overlapping OVs

As mentioned in Section III, our approach differs from that outlined in [8] by allowing overlaps between OVs not in the same contract. Initially built from ensuring routes remain conflict free, the approach employed is to apply a cost function to nodes when building the route. Using the estimated time an aircraft reaches a node along with the distribution of aircraft from any already existing contract

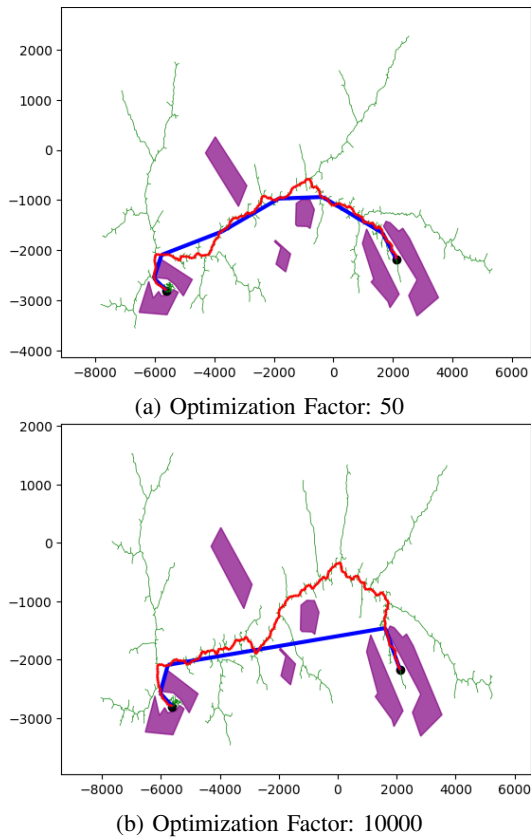


Fig. 2: The RRT\*FND algorithm generating a valid route (red). The route has been further optimized (blue) to decrease the overall distance while avoiding conflicts, this is done based on the RRT-Rope algorithm.

that the node resides in, Equation 8 shows the resultant cost function.

$$\sum_{i=t-n}^{t+n} \sum_{j=1}^k \frac{t-|t-i|}{t} P(S, i, C_j) \quad (8)$$

Where  $t$  is the estimated time of arrival at the node ( $S$ ),  $n$  is a constant used to extend the time query interval to  $[t-n, t+n]$ . The value  $k$  represents the number of OV's that  $S$  resides in. Finally, the weight initial weight value,  $P(S, i, C_j)$ , is obtained from Equation 5.

For any given time  $t$  using this cost function, positional costs can be represented as a heat map, as shown in Figure 3. Costs are calculated in a grid centered around the OV's center. In the example a 10-meter  $\times$  10-meter grid is used. When querying a point  $S$  this results in a query over an area rather than a finite point.

## V. EXPERIMENTS

In this section an evaluation of the performance of the methods employed are carried out. Firstly, the natural 4D point inclusion of the generated OV contracts are examined across three scenarios. The sensitivity OV generation is initial conditions is also evaluated in this section. The performance of the route generation concerning the time to generate, and

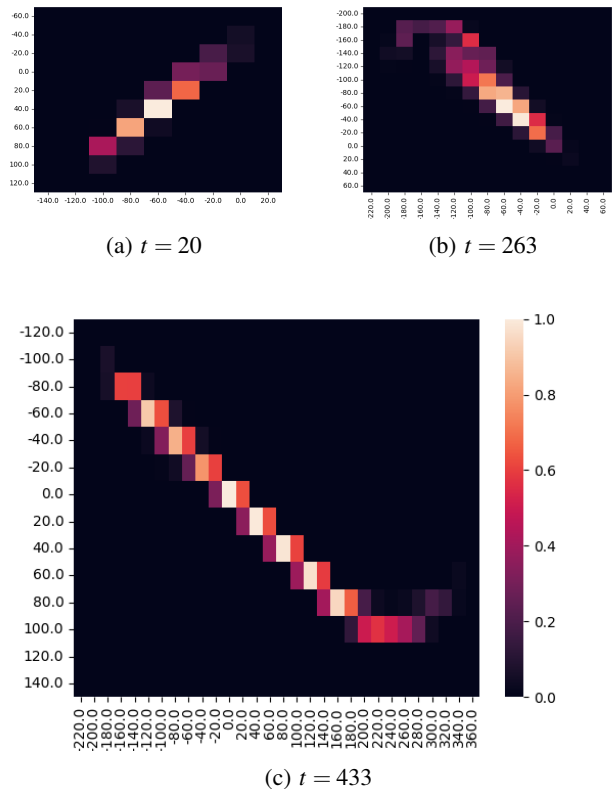


Fig. 3: The costs of 10-meter  $\times$  10-meter areas at  $t = [20, 263, 433]$  respectively. The scale is centered on the applicable OV's where  $(0,0)$  is the center of the OV. The costs have been normalized where 1 is the maximum receivable cost and indicates a higher probability of an aircraft existing there at  $t$ .

the lengths of the initial paths and the optimized paths are also tested in this section.

### A. Evaluation of OV Generation

To evaluate OV generation three predefined routes were used. OV's were then generated for these routes using the method outlined in Section III. Two experiments were designed to evaluate the performance of this approach: The first to test the natural point inclusion of OV's for flights using autopilot; The second to test the sensitivity to initial conditions and the related size of the generated OV's.

1) *Natural point inclusion:* In this experiment simulations were run in BlueSky with 1000 aircraft following the routes and their state data being recorded every second. The recorded data was then compared, both spatially and temporally, with the generated 4D OV's recording the distribution of points that existed within a valid OV at a given time.

The three test scenarios generated tested the natural inclusion of recorded points within the OV contracts. Beyond the autopilot logic implemented in BlueSky the aircraft were not controlled to specifically remain within the OV's. Three scenarios were created for the experiment testing: (1) relatively normal operating over a  $\approx 15$  minute route; (2) a

significantly shorter circular route  $\approx 8$  minute flight time; (3) a complex route with frequent speed and altitude changes and aggressive turns  $> 120^\circ$ , this route was equivalent roughly to a  $\approx 25$  minute flight.

The results can be seen in Table I, and demonstrate high performance within the first two scenarios. The poorer performance in Scenario 3, can be explained through the frequency and aggressiveness of speed changes and heading changes and the time it takes an aircraft to perform the maneuver.

TABLE I: OV point inclusion results

Scenario	Total recorded points	% of points in valid OV
Scenario 1	732102	98.52%
Scenario 2	553717	92.19%
Scenario 3	1176679	79.55%

2) *Sensitivity of OV generation to initial conditions:* In this experiment the initial conditions of the aircraft were altered to provide larger uncertainty. The internal volume of the OVs, measured in kilometers<sup>2</sup> ( $km^2$ ), was then recorded, along with the number of OVs generated.

For this experiment we used the same three test scenarios as mentioned previously. We measured different distributions of speed, position and altitude.

Table II shows the results with variation in the initial speed. The initial position remained constant, and the altitude was between  $[5m, 10m]$ . In Case 1 speeds were generated randomly between  $20ms^{-1}$  and  $24ms^{-1}$  and in Case 2 between  $16ms^{-1}$  and  $26ms^{-1}$ . The results show that, with a larger range of possible initial speeds, the solution generates more OVs and of a larger size. The increase in the number of OVs is likely a result of a larger distribution over the points used when initializing aircraft states from the normal distribution described in Section III-B.1.

TABLE II: OV sensitivity to variation in initial speeds

Scenario	Speed $[20ms^{-1}, 24ms^{-1}]$		Speed $[16ms^{-1}, 26ms^{-1}]$	
	Number of OVs	Mean Area	Number of OVs	Mean Area
Scenario 1	18	0.44	18	1.3
Scenario 2	12	0.1	13	0.1
Scenario 3	28	0.03	29	0.13

In the next experiment, to test sensitivity to initial conditions, changes to the initial positional variation were implemented. Initial starting speed was fixed to  $18ms^{-1}$  but, on the same three scenarios, the area aircraft could be generated was altered. In the first test from the initial starting points, a variation of  $\pm 10m$  was introduced,  $\pm 50m$  for the second and  $\pm 100m$  for the third in any direction. As is expected generated OVs are larger if there is a greater variation in initial starting positions, the results are shown in Table III.

### B. Evaluation Route Generation

To evaluate the performance of candidate route generation the generation time and overall route length were the key

TABLE III: OV sensitivity to variation in starting position

Scenario	Starting Area $\pm 10m$		Starting Area $\pm 50m$		Starting Area $\pm 100m$	
	Number of OVs	Mean Area	Number of OVs	Mean Area	Number of OVs	Mean Area
Scenario 1	18	0.142	18	0.203	18	0.316
Scenario 2	12	0.164	12	0.142	12	0.313
Scenario 3	28	0.032	28	0.038	28	0.046

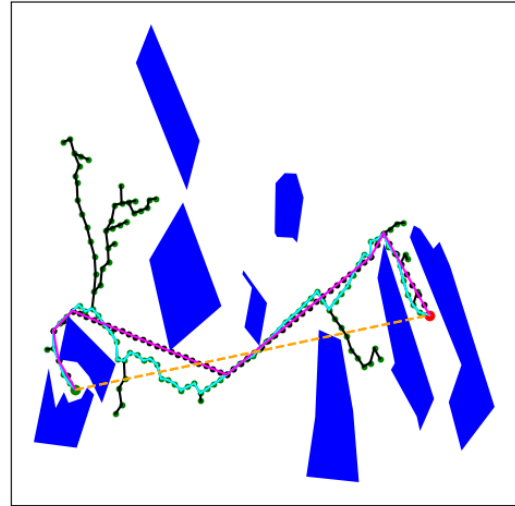


Fig. 4: Example routes generated with the cyan line being the original candidate route ( $10113m$ ), the magenta line is the optimized route ( $9443$ ), and the dashed orange line represents the direct route ( $7761m$ ).

concerning factors. Figure 4 shows the example environment that the routes were generated. The dark blue regions represent static NFZs. Additionally, the candidate route is denoted in cyan, optimized route is colored magenta and the dashed orange line represents the direct distance, which is  $7761m$ .

Two experiments were run to evaluate performance: (1) evaluates the run-time of the route generation, this includes time to optimize the route as well; (2) evaluates the optimization performance, examining how significantly the route can be shortened, using the maximum optimization factor.

1) *Route generation time evaluation:* In this experiment the route generation was run with varying step sizes, maximum distance a node can be from any other node, to evaluate run time. Table IV shows the results of this experiment. Intuitively, the generation time increases exponentially with the resolution of the step size. Pertaining to the *maximum nodes in graph* the  $50m$  resolution step size was unable to generate a valid route with a maximum of 150 nodes in the graph, for this test the maximum number of nodes was increased to 300.

2) *Route optimization evaluation:* To evaluate the performance of the RRT-Rope based optimization, the lengths of

TABLE IV: Time to generate route

	Time (s)	Maximum Nodes in Graph
50 meters	108.82	300
100 meters	19.90	150
150 meters	6.84	150
200 meters	1.85	150

the routes were compared. Again, the resolution of the step size was also considered. Table V shows there appears to be little correlation between the resolution of the step size and the difference in lengths. Each resolution was able to decrease the overall route length by more than 1000m where routes with step sizes 50m and 150m decreased the route length by more than 1500m.

A significant improvement, demonstrated in Figure 2 and Figure 4, is that the optimization significantly decreases the complexity of the route. While the RRT\*FND candidate routes are valid they consist of many sharp or aggressive turns. In flight this could cause significant stress on the vehicle or, increase flight duration significantly. By reducing the path to straight line segments, the optimization not only reduces the overall length but decreases the complexity of the route significantly.

TABLE V: Comparison of candidate and optimized route lengths

	Candidate Length (m)	Optimized Length (m)	$\Delta$ Length (m)
50 meters	11151.01	9369.89	1781.12
100 meters	10975.74	9525.31	1450.43
150 meters	11335.55	9658.40	1677.16
200 meters	11096.91	9836.05	1260.86

## VI. DISCUSSION

### A. Generation of Operational Volumes

In the approach presented in Section III, reachability analysis was performed using the DryVR [26] framework to generate reach tubes. These reach tubes provided the 3D space of the OV. The reachability analysis performed in DryVR leverages a learned *Discrepancy Function* from the sensitivities obtained in the simulation traces. As such, with enough uncertainty or noise in the data, this approach could suffer from the *wrapping effect* [41], resulting in over conservative, non-descriptive OVs. The results in Table II and Table III show the OVs growing in size with more introduced uncertainty. While uncertainty was presented manually, one source of natural uncertainty can be the weather and winds. Including predicted winds into the simulation when generating the OVs will improve the overall model and provide more accurate simulation data to generate the OVs.

An improved method may look at using an analytical approach to reach tube generation. A Lagrangian approach, such as in [27]–[29] has shown to provide tighter bounded reach tubes and claim to not suffer from the *wrapping effect*

[28]. While the DryVR-based approach did not necessarily suffer from the *wrapping effect* the test routes presented were relatively small, larger or more complex routes may result in additional problems.

### B. Route Generation and Deconfliction

The RRT based algorithm used (RRT\*FND) is not known to generate optimal shortest routes. While the approach is suited to a dynamic environment there is limited control on the optimality of the resultant route. As a result, improving this algorithm could be achieved through implementing stricter constraints in where valid nodes can be placed or using an algorithm such as D\* or D\* Lite [13], [42]. Both algorithms provide the dynamic requirement while yielding optimal, shortest-path trajectories. D\* has also been proven to be adaptable to route planning for aircraft in [43], supporting the adoption further.

Additional refinements to either the aircraft positional probability or collision probability within the cost function could also improve the over performance of the system. Presently, the approach only assigns probabilities to within a 10 meter  $\times$  10-meter region of airspace. This presents the problem of routes potentially approaching too closely to potential conflict areas. To improve this, extending regions of high values such that the values diminish in a gradient could discourage the path finding algorithm from approaching too closely to potential conflict regions.

## VII. CONCLUSION

In this paper we presented a novel approach to generating semi-deconflicted routes and accompanying contracts of OVs. We used a reachability analysis method built on the DryVR [26] framework to generate OVs given simulation data obtained in BlueSky [35]. An approach to route generation and deconfliction was given using an adaptation of the RRT algorithm: RRT\*FND. This was then, optimized for shortened distance using the concept of rope-pulling described in [17]. Results demonstrated the ability to generate candidate routes, deconflict them with static NFZs and generate a contract of OVs based on the reachability analysis adapted from DryVR [26]. We also provide an oversight into a potential adaptation of this method that could remove the potential of OV generation to suffer from the wrapping effect by adapting the Lagrangian approach to reachability analysis in [29].

The approach presented in this paper, is intended to be performed pre-flight. However, due to the choice in dynamic path planning algorithm, (RRT\*FND), there is prospect for an in-flight, re-planning approach that largely utilizes the same foundation. This is further reinforced by the path planning and OV generation occurring simultaneously. Additionally, proposed future work will improve both the route generation approach as well as OV generation. And introduce the strategic functionality of deconflicting against existing contracts of OVs.

Furthermore, we intend to develop a tactical, in-flight layer be added to ensure safe separation of en route air vehicles.

We intend to introduce such a tactical system, leveraging the constraints imposed by the aforementioned OVs. That is, a tactical separation assurance component will provide instructions to aircraft to ensure a minimum separation is maintained by air vehicles, both laterally and vertically, and ensure the aircraft remain within their contracted OVs.

## REFERENCES

- [1] B. P. Hill, D. DeCarme, M. Mercalfe, C. Griffin, S. Wiggings, C. Metts, B. Bastedo, M. D. Patterson, and N. L. Medonca, "UAM vision concept of operations (ConOps) UAM maturity level (UML) 4," <https://ntrs.nasa.gov/citations/20205011091>, 12 2020, (accessed Oct. 07, 2022).
- [2] EASA, "Study on the societal acceptance of urban air mobility in europe," <https://www.easa.europa.eu/en/downloads/127760/en>, 05 2021, (accessed Oct. 07, 2022).
- [3] FAA, "Urban air mobility and advanced air mobility," [https://www.faa.gov/uas/advanced\\_operations/urban\\_air\\_mobility](https://www.faa.gov/uas/advanced_operations/urban_air_mobility), 06 2022, (accessed Oct. 07, 2022).
- [4] —, "FAA aerospace forecast fiscal years 2020-2040," <https://www.easa.europa.eu/sites/default/files/dfu/uam-full-report.pdf>, 2020, (accessed Oct. 24, 2022).
- [5] —, "Concept of operations V1.0: Foundation principals, roles and responsibilities, scenario and operational threads," [https://nari.arc.nasa.gov/sites/default/files/attachments/UAM\\_ConOps\\_v1.0.pdf](https://nari.arc.nasa.gov/sites/default/files/attachments/UAM_ConOps_v1.0.pdf), 2020, (accessed Jan. 26, 2023).
- [6] —, "Concept of operations," [https://www.faa.gov/uas/research\\_development/traffic\\_management/media/UTM\\_ConOps\\_v2.pdf](https://www.faa.gov/uas/research_development/traffic_management/media/UTM_ConOps_v2.pdf), 2020, (accessed Sep. 30, 2022).
- [7] SESAR, "Concept of operations for European UTM systems," <https://www.eurocontrol.int/project/concept-operations-european-utm-systems>, 2019, (accessed Sep. 30, 2022).
- [8] C. Hsieh, H. Sibai, H. Taylor, Y. Ni, and S. Mitra, "SkyTrakx: A toolkit for simulation and verification of unmanned air-traffic management systems," in *2021 IEEE International Intelligent Transportation Systems Conference (ITSC)*, 2021, pp. 372–379.
- [9] Catapult, "Implementing an open-access UTM framework for the UK," <https://cp.catapult.org.uk/wp-content/uploads/2021/06/Implementing-an-Open-Access-UTM-Framework.pdf>, 2021, accessed Jan. 11, 2023.
- [10] J. L. Rios, J. Homola, N. Craven, P. Verma, and V. Baskaran, "Strategic deconfliction performance: Results and analysis from the NASA UTM technical capability level 4 demonstration," NASA, Tech. Rep., 2020.
- [11] E. W. Dijkstra, "A note on two problems in connexion with graphs," *Numerische Mathematik*, vol. 1, no. 1, pp. 269–271, 1959.
- [12] P. Hart, N. Nilsson, and B. Raphael, "A formal basis for the heuristic determination of minimum cost paths," *IEEE Transactions on Systems Science and Cybernetics*, vol. 4, no. 2, pp. 100–107, 1968.
- [13] A. Stentz, "Optimal and efficient path planning for partially-known environments," in *Proceedings of the 1994 IEEE International Conference on Robotics and Automation*, 1994, pp. 3310–3317 vol.4.
- [14] S. M. LaValle, "Rapidly-exploring random trees: A new tool for path planning," Computer Science Department, Iowa State University (TR 98–11), Tech. Rep., 1998.
- [15] B. Tong, Q. Liu, and C. Dai, "A RRT FN based path replanning algorithm," in *2019 IEEE 4th Advanced Information Technology, Electronic and Automation Control Conference (IAEAC)*, vol. 1, 2019, pp. 1435–1445.
- [16] O. Adiyatov and H. A. Varol, "A novel RRT-based algorithm for motion planning in dynamic environments," in *2017 IEEE International Conference on Mechatronics and Automation (ICMA)*, 2017, pp. 1416–1421.
- [17] L. Petit and A. L. Desbiens, "RRT-Rope: A deterministic shortening approach for fast near-optimal path planning in large-scale uncluttered 3D environments," in *2021 IEEE International Conference on Systems, Man, and Cybernetics (SMC)*, 2021, pp. 1111–1118.
- [18] S. Razzaq, C. Xydeas, M. E. Everett, A. Mahmood, and T. Alquthami, "Three-dimensional UAV routing with deconfliction," *IEEE Access*, vol. 6, pp. 21 536–21 551, 2018.
- [19] J. Kim and E. Atkins, "Airspace geofencing and flight planning for low-altitude, urban, small unmanned aircraft systems," *Applied Sciences*, vol. 12, no. 2, 2022.
- [20] B. Pang, K. H. Low, and C. Lv, "Adaptive conflict resolution for multi-UAV 4D routes optimization using stochastic fractal search algorithm," *Transportation Research Part C: Emerging Technologies*, vol. 139, p. 103666, 2022.
- [21] H. Liu, X. Li, M. Fan, G. Wu, W. Pedrycz, and P. N. Suganthan, "An autonomous path planning method for unmanned aerial vehicle based on a tangent intersection and target guidance strategy," <https://arxiv.org/abs/2006.04103>, 2020.
- [22] D. Sacharny and T. Henderson, *Strategic Deconfliction*. Cham: Springer International Publishing, 2022, pp. 35–56.
- [23] S. Chaimatanan, D. Delahaye, and M. Mongeau, "Strategic deconfliction of aircraft trajectories," in *ISIATM 2013, 2nd International Conference on Interdisciplinary Science for Innovative Air Traffic Management*, Toulouse, France, Jul. 2013, p. p xxxx.
- [24] X. Tang, Y. Zhang, P. Chen, B. Li, and S. Han, "Strategic deconfliction of 4D trajectory and perturbation analysis for air traffic control and automation system," *Discrete Dynamics in Nature and Society*, vol. 2016, p. 7028305, Sep 2016.
- [25] J. Berling, A. Lau, and V. Gollnick, "European air traffic flow management with strategic deconfliction," in *Operations Research Proceedings 2015*, K. F. Dörner, I. Ljubic, G. Pflug, and G. Tragler, Eds. Cham: Springer International Publishing, 2017, pp. 279–286.
- [26] C. Fan, B. Qi, S. Mitra, and M. Viswanathan, "DryVR: Data-driven verification and compositional reasoning for automotive systems," in *Computer Aided Verification*, R. Majumdar and V. Kunčák, Eds. Cham: Springer International Publishing, 2017, pp. 441–461.
- [27] J. Cyranka, M. A. Islam, S. A. Smolka, S. Gao, and R. Grosu, "Tight continuous-time reachtubes for lagrangian reachability," in *2018 IEEE Conference on Decision and Control (CDC)*, 2018, pp. 6854–6861.
- [28] S. Gruenbacher, J. Cyranka, M. Lechner, M. A. Islam, S. A. Smolka, and R. Grosu, "Lagrangian reachtubes: The next generation," in *2020 59th IEEE Conference on Decision and Control (CDC)*. IEEE, dec 2020.
- [29] S. Gruenbacher, M. Lechner, R. Hasani, D. Rus, T. A. Henzinger, S. Smolka, and R. Grosu, "GoTube: Scalable stochastic verification of continuous-depth models," <https://arxiv.org/abs/2107.08467>, 2021.
- [30] C. Fan, J. Kapinski, X. Jin, and S. Mitra, "Simulation-driven reachability using matrix measures," *ACM Trans. Embed. Comput. Syst.*, vol. 17, no. 1, dec 2017.
- [31] J. Maidens and M. Arcak, "Reachability analysis of nonlinear systems using matrix measures," *IEEE Transactions on Automatic Control*, vol. 60, no. 1, pp. 265–270, 2015.
- [32] G. Zhu and P. Wei, *Low-Altitude UAS Traffic Coordination with Dynamic Geofencing*.
- [33] M. Stevens and E. Atkins, "Geofence definition and deconfliction for UAS traffic management," *IEEE Transactions on Intelligent Transportation Systems*, vol. 22, no. 9, pp. 5880–5889, 2021.
- [34] S. Balachandran, A. Narkawicz, C. A. Muñoz, and M. C. Consiglio, "A path planning algorithm to enable well-clear low altitude UAS operation beyond visual line of sight," in *Twelfth USA/Europe Air Traffic Management Research and Development Seminar (ATM2017)*, 2017.
- [35] J. Hoekstra and J. Ellerbroek, "BlueSky ATC simulator project: an open data and open source approach," 2016.
- [36] J. Sun, J. M. Hoekstra, and J. Ellerbroek, "OpenAP: An open-source aircraft performance model for air transportation studies and simulations," *Aerospace*, vol. 7, no. 8, p. 104, 2020.
- [37] Airbus, "Vahana: Our single-seat eVTOL demonstrator," <https://www.airbus.com/en/urbanairmobility/cityairbus-nextgen/vahana>, (accessed Nov. 12, 2022).
- [38] P. Pradeep, "Arrival management for eVTOL aircraft in on-demand urban air mobility," Ph.D. dissertation, Iowa State University, 05 2019.
- [39] J. P. Snyder, "Map projections: A working manual," U.S. Department of the Interior, Washington, D.C., Tech. Rep., 1987, report.
- [40] L. M. Bugayevskiy and J. Snyder, *Map Projections - A Reference Manual*. CRC Press, 1995.
- [41] A. Neumaier, *The Wrapping Effect, Ellipsoid Arithmetic, Stability and Confidence Regions*. Vienna: Springer Vienna, 1993, pp. 175–190.
- [42] S. Koenig and M. Likhachev, "D\* Lite," *AAAI Conference of Artificial Intelligence (AAAI)*, pp. 476–483, 2002.
- [43] S. Majumder and M. S. Prasad, "Three dimensional D\* algorithm for incremental path planning in uncooperative environment," in *2016 3rd International Conference on Signal Processing and Integrated Networks (SPIN)*, 2016, pp. 431–435.